

1 **Reduction of Pacific double-ITCZ bias by convection**
2 **parameterization in NCAR CESM2.2**

6 Xiaoliang Song and Guang J. Zhang
7 Scripps Institution of Oceanography
8 La Jolla, CA 92093-0230

11 **For publication in *J. Adv. Model. Earth Syst.***

12 **February 2024**

21 **Key Points:**

- 22 • Modifications to the closure in convection parameterization scheme greatly reduce the
23 double-ITCZ bias in all seasons in CESM2.2
- 24 • Convection scheme can modulate the tropical atmosphere-ocean feedback processes,
25 through which it influences the SST and double-ITCZ biases
- 26 • Surface heat flux changes play a limited role in reducing the SST and double-ITCZ biases

31 Corresponding author address: Dr. Xiaoliang Song, Scripps Institution of Oceanography, La Jolla,
32 CA 92093-0230; e-mail: xisong@ucsd.edu.

33

Abstract

34 The impact of convective closure on the double-ITCZ bias in the NCAR CESM2.2 is
35 investigated in this study. The standard CESM2.2 simulates a remarkable double-ITCZ bias in the
36 central and eastern Pacific, especially in boreal winter and spring. Modifications to the closure in
37 convection parameterization scheme greatly reduce the double-ITCZ bias in all seasons,
38 demonstrating that convection parameterization can substantially influence the double-ITCZ bias
39 in CESM2.2. Further analyses suggest that convection parameterization can modulate the tropical
40 atmosphere-ocean feedback processes, through which it influences the SST in the southern ITCZ
41 region and hence the double-ITCZ bias. The changes in the upper ocean temperature advection
42 induced by modified convective closure plays important roles in reducing the warm SST bias and
43 double-ITCZ precipitation bias in the southern ITCZ region. The modified convective closure
44 improves the low-level cloud and shortwave cloud radiative forcing in the southeastern Pacific.
45 However, surface heat flux plays only a limited role in reducing warm SST bias and double ITCZ
46 bias because the impacts of shortwave radiation changes are largely canceled by changes in
47 longwave radiation and latent heat flux.

48

49

50

51

52

53

54

55

56

57

58

Plain language summary

59

60 Despite decades of model development, the large-scale distribution of precipitation
61 simulated by most of coupled global climate models (GCMs) still displays a remarkable double-
62 intertropical convergence zone (ITCZ) bias over the tropical Pacific Ocean. Observations show
63 asymmetrical distribution of precipitation with respect to the equator in the central and eastern
64 Pacific with one intense ITCZ precipitation band north of the equator all year-round and a much
65 weaker zonal rain band south of the equator (southern ITCZ) only in boreal spring. However,
66 coupled GCMs tend to simulate overly strong southern ITCZ rain band, resulting in double-ITCZ
67 bias in annual mean precipitation. In this study, we investigate the impact of convection
68 parameterization scheme on the double-ITCZ bias in the NCAR Community Earth System Model,
69 version 2.2 (CESM2.2). The standard CESM2.2 simulates a remarkable double-ITCZ bias in the
70 central and eastern Pacific. Modifications to the closure in convection parameterization scheme
71 greatly reduce the double-ITCZ bias, demonstrating that the convection parameterization can
72 substantially influence the double-ITCZ bias in CESM2.2. Further analyses suggest that the
73 convection parameterization can modulate the tropical atmosphere-ocean feedback processes,
74 through which it influences the upper ocean temperature advections, sea surface temperature, and
75 hence precipitation in the southern ITCZ region.

76

77

78

79

80

81 **1. Introduction**

82 Despite decades of climate model development, the large-scale distribution of precipitation
83 simulated by coupled global climate models (GCMs) still displays significant biases over tropical
84 oceans. Observations show a single zonal intertropical convergence zone (ITCZ) precipitation
85 band north of the equator all year-round in the central and eastern tropical Pacific, with a much
86 weaker zonal rain band south of the equator (southern ITCZ) observed only in boreal spring (Zhang,
87 2001). However, coupled GCMs tend to simulate overly strong southern ITCZ rain band for more
88 than half of the year in the central and eastern tropical Pacific, resulting in the appearance of a
89 double-ITCZ bias in annual mean precipitation (Mechoso et al., 1995; Lin, 2007; Zhang et al.,
90 2015; Tian and Dong 2020). The double-ITCZ bias is especially remarkable in boreal winter and
91 spring.

92 In the past decades, a number of hypotheses have been proposed for the possible root causes
93 of the double-ITCZ bias. However, even today, there is still no consensus among scientists on the
94 formation mechanism of the double-ITCZ bias. Early studies attributed the double-ITCZ bias to
95 the local warm SST bias in the southeastern Pacific associated with the underestimated stratus
96 cloud off the west coast of South America (Ma et al. 1996; Yu and Mechoso, 1999). Sensitivity
97 experiments with modified cloud cover show the alleviation of double-ITCZ bias in the southern
98 Pacific, however, the cold and dry tongue biases in SST and precipitation were exacerbated. It was
99 later argued that the tropical double-ITCZ bias may be remotely caused by extratropical biases in
100 cloud and radiation over the Southern Ocean through energetic constraint (Hwang and Frierson,
101 2013). However, a few follow-up studies disagree on this remote mechanism (e.g., Kay et al., 2016;
102 Hawcroft et al., 2017). Recently, Kim et al. (2022) explored the teleconnection mechanism from
103 the Southern Ocean to the Tropical Pacific first suggested by Mechoso et al. (2016). They argued

104 that the strength of teleconnection is strongly modulated by the subtropical stratocumulus cloud-
105 SST feedback in the southeastern tropical Pacific. The overly weak subtropical low cloud feedback
106 in GCMs results in a much weaker contribution from extratropical biases to tropical double-ITCZ
107 bias. Kawai et al. (2021) investigated the relationship between radiation bias over the Southern
108 Ocean and the tropical double-ITCZ bias in Meteorological Research Institute Earth System Model
109 version 2.0 (MRI-ESM2.0). They found that the modifications in stratocumulus scheme, shallow
110 convection scheme, and cloud microphysics parameterization can reduce the radiation bias over
111 the Southern Ocean. Correspondingly, the tropical double-ITCZ bias was also reduced to some
112 extent. However, they also found that the double-ITCZ bias was still present even when the
113 radiation bias was eliminated over the Southern Ocean, indicating that other processes may be
114 responsible for the double-ITCZ bias. They hypothesized that deep convection and shallow
115 convection schemes may play important roles. Bypassing the cloud-SST feedback issues by
116 prescribing SST with observations in the southeastern subtropical Pacific in a coupled GCM
117 CESM1, Song and Zhang (2016) found reduced double-ITCZ biases in the annual mean. However,
118 the seasonal evolution still showed large precipitation biases in boreal spring. Lee et al. (2022)
119 investigated the causes of double-ITCZ bias in GFDL CM2.1. Their analyses suggest the zonal-
120 mean diagnostics poorly represent the spatial pattern of precipitation bias in the tropical pacific
121 (e.g., double-ITCZ). They demonstrated that tropical precipitation bias is mostly locally driven
122 from the tropical SST bias. By analyzing the severity of the double-ITCZ bias in CMIP5 models,
123 Xiang et al. (2017) also revealed statistical evidence that the largest source of the double-ITCZ
124 bias is from the tropics. Zhou and Xie (2017) analyzed the severity of the double-ITCZ bias in
125 CMIP5 models and found that this bias is closely correlated with the land surface temperature bias.

126 As ITCZ precipitation is largely produced by deep convective clouds, deep convection
127 parameterization schemes have also been considered as a major cause for double-ITCZ bias. Zhang
128 and Wang (2006) examined the impact of a revised closure (Zhang, 2002) of the Zhang-McFarlane
129 convection scheme (Zhang & McFarlane, 1995) in the NCAR Community Climate System Model,
130 version 3 (CCSM3). They found that the spurious southern ITCZ precipitation band in the central
131 equatorial Pacific is generally eliminated in boreal summer with the revised convective closure.
132 As a result, the annual-mean double-ITCZ biases in precipitation, sea surface temperature (SST),
133 wind stress, and upper ocean currents are all significantly reduced through a complex coupled
134 feedback between convection, surface wind, upper-ocean currents, and SST (Song and Zhang,
135 2009; Zhang & Song, 2010). It should be noted that the double ITCZ biases in boreal winter and
136 spring still exist in the CCSM3 with the revised convective closure. Alleviating the double-ITCZ
137 bias in boreal winter and spring remains a challenging task. Zhang et al. (2019) provided a
138 comprehensive review of the roles of the Southern Ocean radiation bias, southeastern Pacific cloud
139 bias and convection parameterization in double ITCZ in GCMs.

140 Significant model developments greatly improved the capability and performance of the
141 NCAR global climate model, with the Community Climate System Model (CCSM) upgraded to
142 the Community Earth System Model (CESM). However, double-ITCZ biases still persist. To
143 investigate the role of convection parameterization in the formation of double-ITCZ biases in the
144 CESM, Song and Zhang (2018) further examined the impact of the revised convective closure
145 (Zhang, 2002) on double-ITCZ biases in NCAR CESM1.2.1. They found that the double-ITCZ
146 biases are generally eliminated in boreal summer and autumn but persist in boreal winter and
147 spring when the revised convective closure is used, similar to the impact documented in Song and
148 Zhang (2009). Song and Zhang (2018) then further implemented improvements in the trigger

149 function and cloud model of the ZM convection scheme into CESM1.2.1 and found that the
150 double-ITCZ biases are largely eliminated in all seasons with the improved convection scheme,
151 although there is still a dry tongue bias over the equator. Their analyses show that other possible
152 contributors, such as cloud biases off the western coast of South America and over the Southern
153 Ocean, are barely changed in their simulations, leading to the conclusion that the convection
154 scheme is the primary contributor to the formation of double-ITCZ biases in the CESM1.2.1.

155 Woelfle et al. (2019) investigated the evolution of double-ITCZ biases in 10 intermediate
156 model versions through the development from CESM1 to CESM2. They found that the double-
157 ITCZ biases in the southeast Pacific in CESM2 are greatly reduced as compared to its previous
158 version (CESM1), although the global mean ITCZ position and cold tongue bias do not exhibit
159 significant improvement. The evolution of the double-ITCZ biases across development
160 simulations suggests that the improved ITCZ in the southeast Pacific can be associated with the
161 reduction of warm bias in the underlying SST, which can be attributed to increases in low cloud
162 cover and associated cloud radiative forcing. The improved cloud simulation in the southeast
163 Pacific is further attributed to changes in the cloud microphysics scheme, which decrease drizzle
164 rates and increase cloud fraction and lifetime. The analysis of drizzling bias (i.e., too frequent
165 drizzling) and double-ITCZ bias in CMIP5 and CMIP6 models (Zhou et al. 2022) also supports
166 this mechanism. The authors argued that the excessive drizzling rain in the stratocumulus region
167 can lead to fewer low-level clouds, which increase the incoming solar radiation and thus the warm
168 SST bias in the southeastern Pacific.

169 Ma et al. (2023) assessed the double-ITCZ bias in the models participating in the Coupled
170 Model Intercomparison Project Phase 6 (CMIP6) and found that the models with relatively low

171 double-ITCZ bias tend to restrain the frequency of deep convection effectively, highlighting that
172 the convective process is crucial for mitigating the double ITCZ bias in coupled GCMs.

173 In this study, we examine the impact of convective closure on double-ITCZ bias in the
174 newest version of NCAR CESM, CESM2.2 (Herrington et al. 2022). It is shown that the revised
175 convective closure (Zhang 2002) eliminates the double-ITCZ biases not only in boreal winter and
176 spring but also in summer and autumn in CESM2.2, which is different from its performance in
177 CESM1.2.1, where it can only eliminate the double-ITCZ biases in boreal summer and autumn,
178 indicating that changes in other model parameterizations can modulate the impact of the
179 convection scheme and hence influence the formation of double-ITCZ biases. Since the revised
180 convective closure can eliminate double-ITCZ bias in all seasons, it provides us a good opportunity
181 to understand how convection parameterization influences the double-ITCZ biases in CESM.
182 Detailed feedback analyses are performed to enhance our understanding on this issue.

183 The rest of paper is organized as follows: Section 2 briefly describes the model, convective
184 closure, simulations, and observational data. Section 3 presents the impacts of the convective
185 closure on the double-ITCZ bias in the CESM2.2. Section 4 analyzes coupled feedback mechanism
186 through which the convective parameterization influences the double-ITCZ biases. Section 5
187 summarizes the results and conclusions.

188 **2. Model, experiments, and data**

189 **a. Model and the revised convective closure**

190 The NCAR Community Earth System Model, version 2.2 (CESM2.2), is used in this study.
191 The CESM2.2 is a fully coupled, state-of-the-art, global climate model. The component models
192 include the Community Atmosphere Model version 6 (CAM6, Danabasoglu et al., 2020), the

193 Community Land Model version 5 (CLM5), the Los Alamos sea ice model version 5 (CICE5), the
194 Parallel Ocean Program version 2 (POP2), Community Ice Sheet Model (CISM) version 2.1, the
195 Model for Scale Adaptive River Transport (MOSART), and NOAA WaveWatch-III ocean surface
196 wave prediction model. In the CAM6, the moist boundary layer, shallow convection, and cloud
197 macrophysics are parameterized with the Cloud Layers Unified by Binormals (CLUBB) scheme,
198 and the large-scale cloud and precipitation processes are parameterized with an improved two-
199 moment prognostic bulk cloud microphysics scheme (MG2, Gettelman and Morrison 2015). The
200 Zhang and McFarlane convection scheme with a dilution approximation for the calculation of
201 convective available potential energy (CAPE, Neale et al. 2008) is used for deep convection.

202 The default ZM convection scheme in CESM2.2 employs a CAPE-based closure, which
203 assumes that convection acts to consume CAPE in a specified relaxation time period. Therefore,
204 the convection intensity is proportional to the amount of CAPE. Zhang (2002) proposed a revised
205 closure which assumes that the CAPE generation rate by large-scale forcing in the free troposphere
206 can be approximately balanced by the CAPE consumption rate due to convection. That means the
207 convection intensity is proportional to the CAPE generation rate instead of the amount of CAPE.
208 Song and Zhang (2009, 2018) demonstrated that this closure can reduce the double-ITCZ bias in
209 boreal summer in CCSM3 and CESM1.2.1, respectively. In this study, we employ this revised
210 closure in the ZM convection scheme in CESM2.2 to investigate its impact on the double-ITCZ
211 bias. In the experiment, although we do not modify the original CAPE-based trigger in the ZM
212 convection scheme, when the dCAPE closure is applied in the convection scheme, it in effect also
213 serves as a trigger. This is because when $dCAPE \leq 0$ the cloud base mass flux is zero, meaning
214 that convection is not triggered. A dCAPE-based trigger was used in E3SM by Xie et al. (2019).

215 **b. Simulations**

216 Two 11-year fully coupled simulations of CESM2.2 are conducted: one using the default
217 version of the ZM convection scheme (referred to as the CTL run), and another using the ZM
218 scheme with the revised closure (referred to as the RZM run). Both simulations employed B1850
219 component setting and f09_g17 grid configuration, which means that a $0.9^\circ \times 1.25^\circ$ resolution
220 (latitude x longitude) is used in both atmospheric and land models. Version 7 of 1° Greenland Pole
221 ocean/ice grid is used for ocean and sea ice models. The 5-year averages for years 7–11 are used
222 to analyze the double-ITCZ bias in this study.

223 To identify the contribution of air-sea feedback in the formation of double-ITCZ bias and
224 understand the impact of the revised convective closure on the atmospheric response to fixed SST,
225 a set of 7-year Atmospheric Model Intercomparison Project (AMIP) type simulations are
226 conducted using the CESM2.2. The AMIP simulation with the standard ZM scheme is referred to
227 as CTL_amip, whereas the simulation using the revised closure in ZM convection scheme is
228 referred to as RZM_amip. Both simulations employed F1850 component setting and f09_f09 grid
229 configuration, which means the atmosphere model is driven by forcing (e.g., SST) in 1850 with a
230 $0.9^\circ \times 1.25^\circ$ resolution (latitude x longitude). The 5-year averages for years 3–7 are used in the
231 analyses.

232 **c. Observational data**

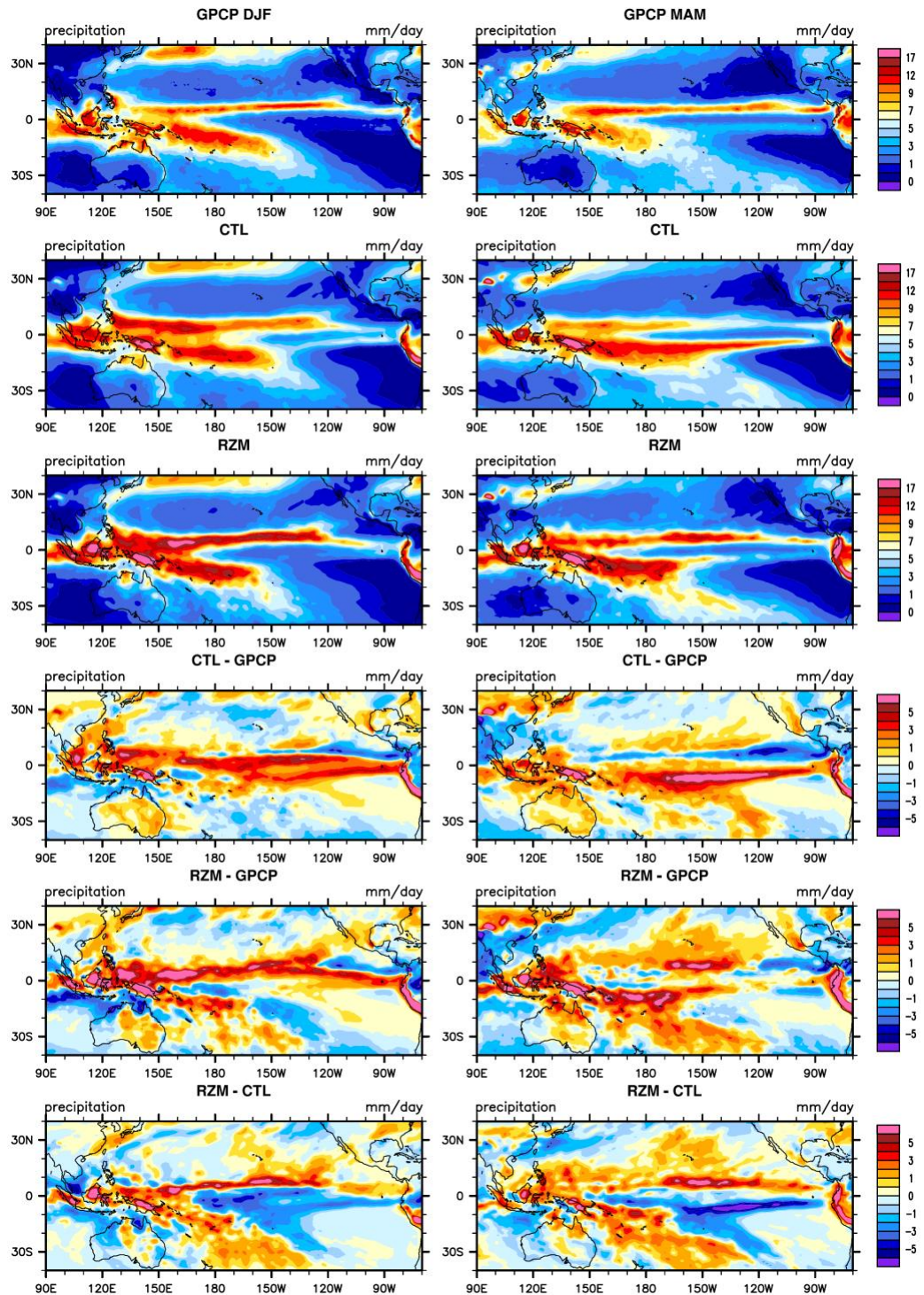
233 The Global Precipitation Climatology Project (GPCP) Version 3.2 precipitation analysis
234 from 1983 to 2021 (Huffman et al. 2023), SST from the Hadley Centre Sea Ice and Sea Surface
235 Temperature (HadISST) dataset between 1870 and 1900 (Rayner et al. 2003), the monthly mean
236 meridional/zonal wind speed and pressure vertical velocity from ECMWF Reanalysis v5 (ERA5)
237 (Hersbach et al. 2020) from 1979 to 2019, GCM-Oriented CALIPSO Cloud Product (CALIPSO-

238 GOCCP, Chepfer et al. 2010) from 2007 to 2010, and Clouds and the Earth's Radiant Energy
239 System (CERES) Energy Balanced and Filled (EBAF) from 2001-2018 (Kato et al. 2018) are
240 used in the simulation evaluation.

241 **3. Impacts of the convective closure on the double ITCZ bias**

242 Figure 1 shows precipitation from the GPCP observation, the CTL and RZM simulations,
243 along with their differences, averaged in boreal winter (December, January, February, DJF) and
244 spring (March, April, May, MAM), respectively, when the double-ITCZ biases are most prominent.
245 In winter, the GPCP observations show a southeastward SPCZ rain band south of the equator and
246 only one zonal ITCZ rain band north of the equator, forming a strikingly asymmetric structure
247 relative to the equator. Precipitation of $>4 \text{ mm day}^{-1}$ is confined to the west of 150°W between
248 $2^\circ\text{S}-10^\circ\text{S}$. CTL simulates two zonal rain bands straddling the equator across the Pacific, with
249 precipitation of $>4 \text{ mm day}^{-1}$ extending to the west coast of south America between $2^\circ\text{S}-10^\circ\text{S}$,
250 demonstrating a typical double-ITCZ bias. Compared to its previous version (CESM1.2.1, Song
251 and Zhang 2018, Fig.1c), CESM2.2 does not simulate a notable dry tongue bias over the equator.
252 The overestimated precipitation in the southern ITCZ region between 120°W and 150°W is also
253 reduced, indicating the double-ITCZ bias was mitigated due to model development from CESM1
254 to CESM2.2. With the revised closure, the spurious southern ITCZ rain band in the central and
255 eastern Pacific is generally eliminated in the RZM simulation. Precipitation of $>4 \text{ mm day}^{-1}$ is
256 confined to the west of 150°W between $2^\circ\text{S}-10^\circ\text{S}$. Precipitation of $< 4 \text{ mm day}^{-1}$ is extended to
257 180° near the equator. Both of these changes lead RZM to good agreement with GPCP
258 observations. The difference between CTL and GPCP clearly shows that CTL simulates a spurious
259 southern ITCZ rain band in central and eastern Pacific with overestimated precipitation up to 5
260 mm day^{-1} . The RZM reduces the positive precipitation bias in the central and eastern Pacific

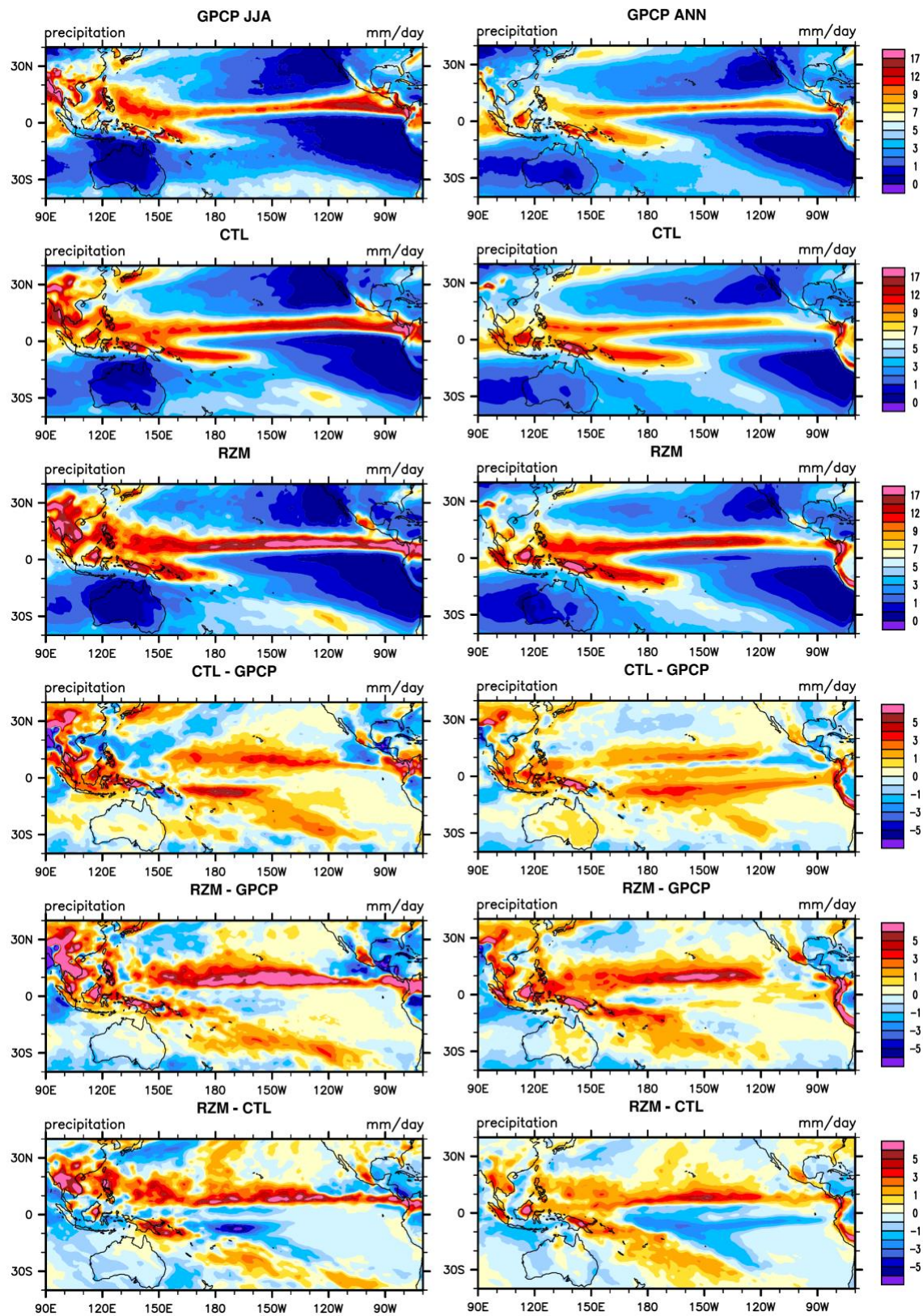
261 between 2°S and 10°S by up to 4 mm day⁻¹, resulting in the double-ITCZ bias being largely
262 eliminated.



263
264 Figure 1 Precipitation (mm day⁻¹) from GPCP, CTL, RZM and their difference for DJF (left
265 column) and MAM (right column).

266 In boreal spring, GPCP observation shows two parallel zonal rain bands in central and
267 eastern Pacific, with the southern ITCZ being much weaker than the northern ITCZ. The
268 precipitation in the southern ITCZ region is generally below 4 mm day^{-1} . CTL simulates an
269 opposite precipitation distribution compared to observation, with a much stronger southern ITCZ
270 rain band than the northern ITCZ. The simulated precipitation is up to 12 mm day^{-1} in the southern
271 ITCZ region, which contributes significantly to the double-ITCZ bias in annual mean precipitation.
272 The RZM generally reproduces the observed asymmetric distribution of precipitation in central
273 and eastern Pacific. The simulated precipitation is about 4 mm day^{-1} in southern ITCZ the eastern
274 Pacific, although it still slightly overestimates the southern ITCZ precipitation in central pacific.
275 The difference between CTL and GPCP clearly shows that CTL overestimates precipitation by up
276 to 7 mm day^{-1} in southern ITCZ and underestimates precipitation by up to 6 mm day^{-1} in northern
277 ITCZ in central and eastern Pacific. The RZM reduces the positive precipitation bias between 2°S
278 and 10°S by up to 7 mm day^{-1} and increases negative precipitation bias between 2°N - 10°N by up
279 to 7 mm day^{-1} in central and eastern Pacific, indicating that the double-ITCZ bias in spring is largely
280 eliminated as well.

281 In boreal summer (June, July, and August, JJA), the observed SPCZ precipitation (Fig.2a)
282 retracts into the western Pacific with precipitation of $>7 \text{ mm day}^{-1}$ located west of 170°E between
283 2°S and 10°S . However, the CTL still tends to simulate too zonally elongated southern Pacific rain
284 band with precipitation of $> 7 \text{ mm day}^{-1}$ extending eastward to 160°W between 2°S and 10°S ,
285 resulting in double-ITCZ bias in the western Pacific. Note that the double-ITCZ bias simulated by
286 its previous version (CESM1.2.1,) in summer (Song and Zhang 2018, Fig.2f) is pronounced in
287 both the western and central Pacific, demonstrating that model development from CESM1 to
288 CESM2.2 substantially mitigated the double-ITCZ bias in the central Pacific in the



289

290 Figure 2 Same as Fig. 1 but for JJA (left column) and annual mean (ANN, right column).

291 summer season. The SPCZ precipitation simulated by RZM is in good agreement with GPCP
292 observations with precipitation of $> 7 \text{ mm day}^{-1}$ west of 180° , indicating that the revised convective
293 closure can generally eliminate double-ITCZ bias in summer as well. The impact of revised
294 convective closure on double-ITCZ bias in boreal autumn is similar to that in summer (not shown).
295 As a result, the RZM completely eliminates the double-ITCZ bias in the central and eastern Pacific
296 in annual mean precipitation. The annual-mean precipitation of $> 3 \text{ mm day}^{-1}$ simulated by RZM
297 between 2°S and 10°S is located west of 145°W , which is in good agreement with the observations.
298 In contrast, the annual-mean precipitation of $> 3 \text{ mm day}^{-1}$ simulated by CTL between 2°S and
299 10°S is extended all the way to 90°W , resulting in remarkable double-ITCZ biases in the central
300 and eastern Pacific.

301 To quantitatively evaluate the changes in double-ITCZ bias, we calculate the Pacific ITCZ
302 pattern index, which is defined as the difference between the northern ITCZ (2°N - 10°N , area-
303 averaged) precipitation and the southern ITCZ (2°S - 10°S , area-averaged) precipitation normalized
304 by the tropical mean precipitation (10°S - 10°N) in the central and eastern Pacific over 85°W -
305 160°W . This pattern index reflects the interhemispheric asymmetry in ITCZ precipitation in the
306 central and eastern Pacific, where the double-ITCZ bias is most prominent. Similar global index
307 has been widely used in past research (e.g., Hwang & Frierson, 2013; Tian and Dong, 2020). Table
308 1 shows the Pacific ITCZ pattern index from GPCP, RZM and CTL simulations. Positive values
309 mean that the northern ITCZ precipitation is stronger than the southern ITCZ. The ITCZ pattern
310 index from GPCP reveals that the northern ITCZ is stronger than the southern ITCZ all year-round
311 in observations, with weaker interhemispheric asymmetry in boreal winter and spring. However,
312 CTL simulates a negative ITCZ pattern index in spring, reflecting that the southern ITCZ
313 precipitation is stronger than its northern counterpart. CTL also simulates a very weak ITCZ

314 pattern index in winter. As a result, the annual mean ITCZ pattern index simulated by CTL is only
315 about half of the observation, indicating a large double-ITCZ bias because the southern ITCZ
316 precipitation simulated by CTL is more comparable to the northern ITCZ. RZM successfully
317 reproduces the observed ITCZ pattern index, especially in annual mean precipitation,
318 demonstrating that the double-ITCZ bias is generally eliminated with the revised convective
319 closure. Although the widely used ITCZ pattern index can represent the interhemispheric
320 asymmetry of ITCZ precipitation, it does not directly assess the southern ITCZ precipitation bias
321 and double-ITCZ bias. We further define a double-ITCZ bias index as the ratio of southern ITCZ
322 (2°S-10°S) precipitation relative to northern ITCZ (2°N-10°N) precipitation in the central and
323 eastern Pacific over 85°W-160°W. When there is only a single ITCZ, the double-ITCZ bias index
324 will be very close to zero, while when there is a double-ITCZ the double-ITCZ bias index will be
325 close to or larger than one. Table 2 shows the double-ITCZ bias index from GPCP, RZM and CTL
326 simulations. The double-ITCZ bias index from GPCP reveals that the southern ITCZ precipitation
327 is only about 10% of northern ITCZ precipitation in summer and fall and increased to 44% in
328 spring. In annual mean precipitation, the southern ITCZ is about 21% of northern ITCZ. The
329 double-ITCZ bias index simulated by CTL is about three times as large as that in observations in
330 winter and spring, indicating a remarkable double-ITCZ bias. Again, RZM successfully
331 reproduces the observed double-ITCZ bias index, not only in annual mean but also for all seasons,
332 demonstrating that the double-ITCZ bias is generally eliminated with the revised convective
333 closure. However, although the revised closure significantly improves the simulation of the
334 asymmetric distribution of ITCZ precipitation with respect to the equator, it generally tends to
335 simulate stronger ITCZ precipitation than observed.

336

337

Table 1. Pacific ITCZ pattern index from GPCP, RZM and CTL simulations.

ITCZ pattern index	ANN	DJF	MAM	JJA	SON
GPCP	1.545	1.481	0.897	1.948	2.128
RZM	1.544	1.333	0.803	2.087	2.013
CTL	0.828	0.522	-0.377	1.767	1.914

338

339

Table 2. Double-ITCZ bias index from GPCP, RZM and CTL simulations.

Double-ITCZ bias index	ANN	DJF	MAM	JJA	SON
GPCP	0.21	0.22	0.44	0.11	0.07
RZM	0.20	0.23	0.47	0.07	0.09
CTL	0.46	0.59	1.41	0.15	0.11

340

341

342

343

344

345

346

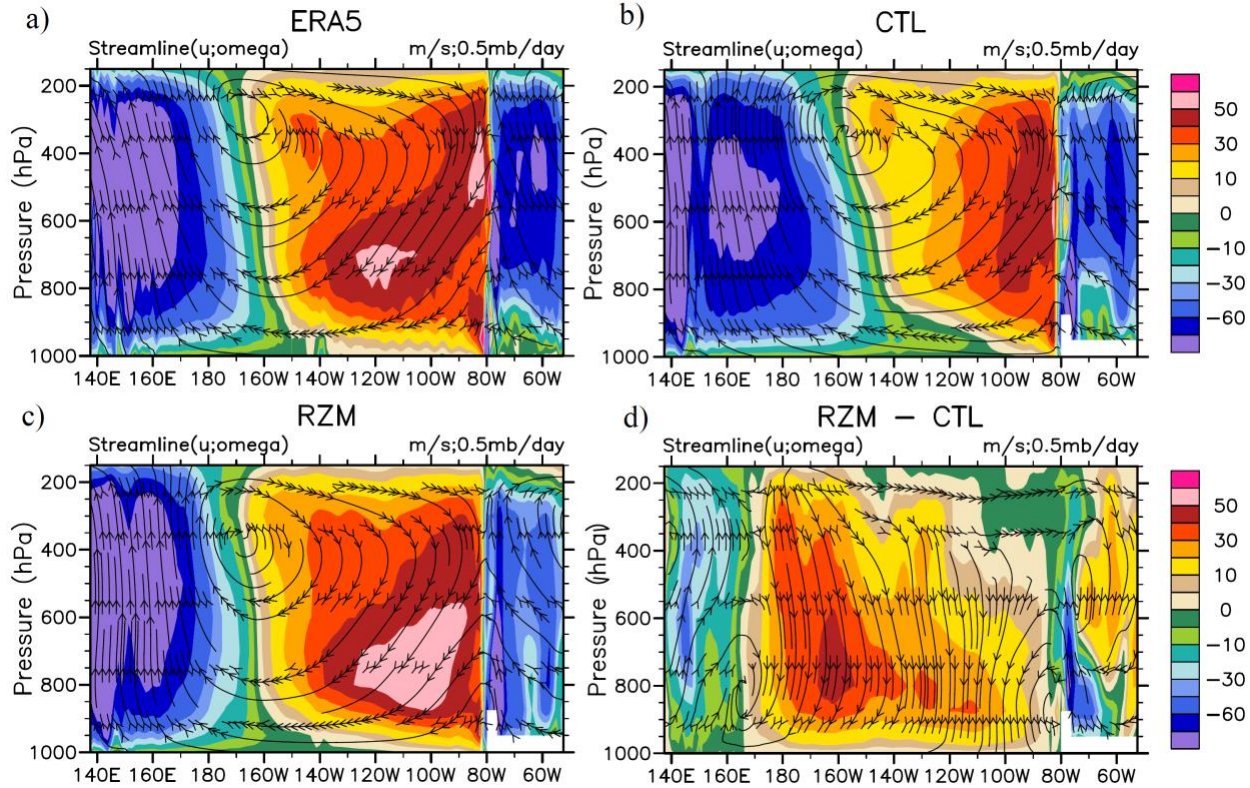
347

348

349

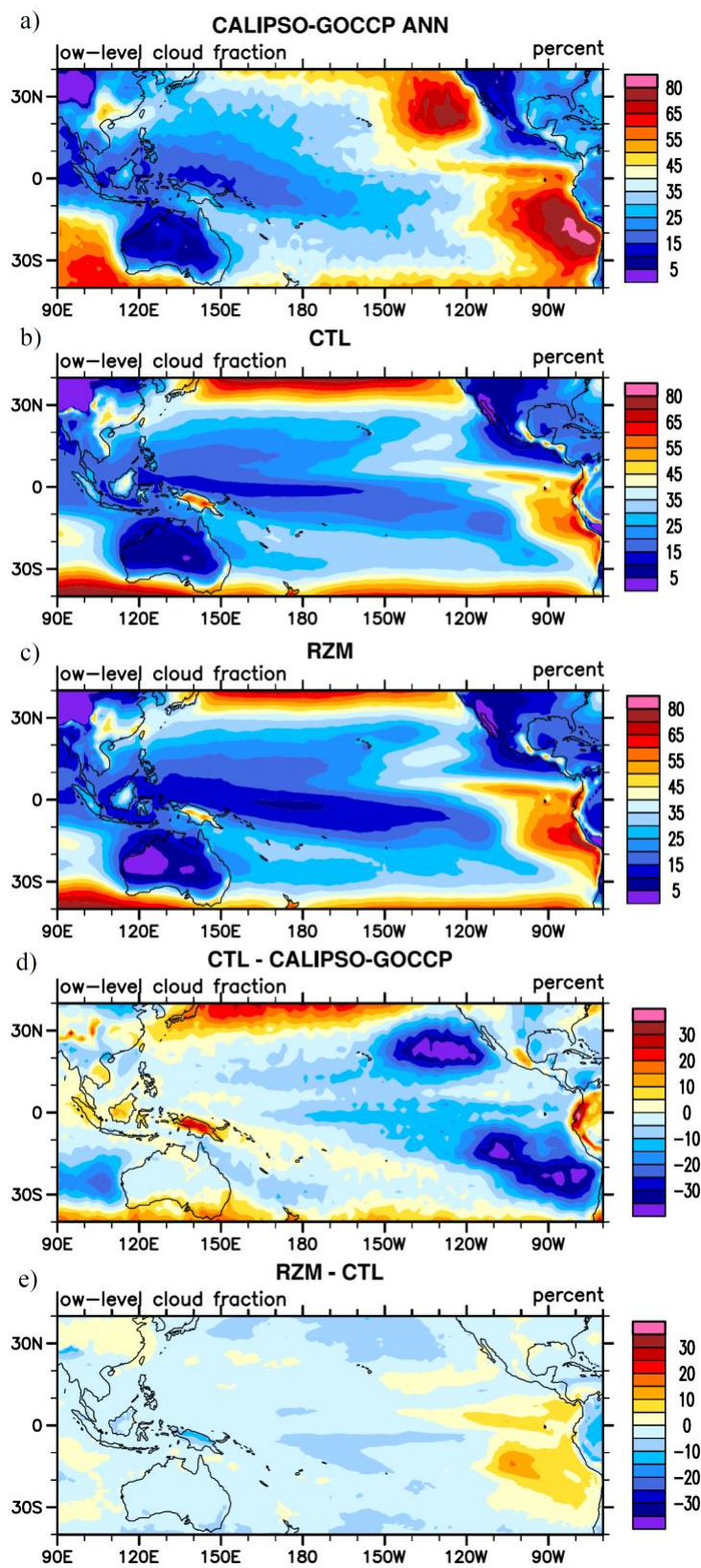
Convection-circulation interaction is one of the most important processes through which convection parameterization schemes influence climate simulation. Fig.3 presents the annual mean vertical velocity (shaded) and zonal circulation (streamline) averaged over the southern ITCZ region (2°S - 10°S) from ERA5, CTL and RZM simulations. ERA5 shows a typical Walker circulation with deep ascending motion west of 170°W , deep descending motion east of 160°W , and easterly wind in the lower troposphere. Corresponding to the zonally elongated southern ITCZ rain band, the deep ascending motion regime in CTL is extended eastward to 160°W , with the regime of shallow ascending motion extending to 100°W . RZM successfully reproduces the observed Walker Circulation, with deep ascending motion west of 170°W and deep descending

350 motion east of 160°W . The difference between RZM and CTL clearly shows that the modified
 351 convective closure induces increased descending motion in the central and eastern Pacific, stronger
 352 ascending motion in the western Pacific, and enhanced easterly winds in the lower troposphere.



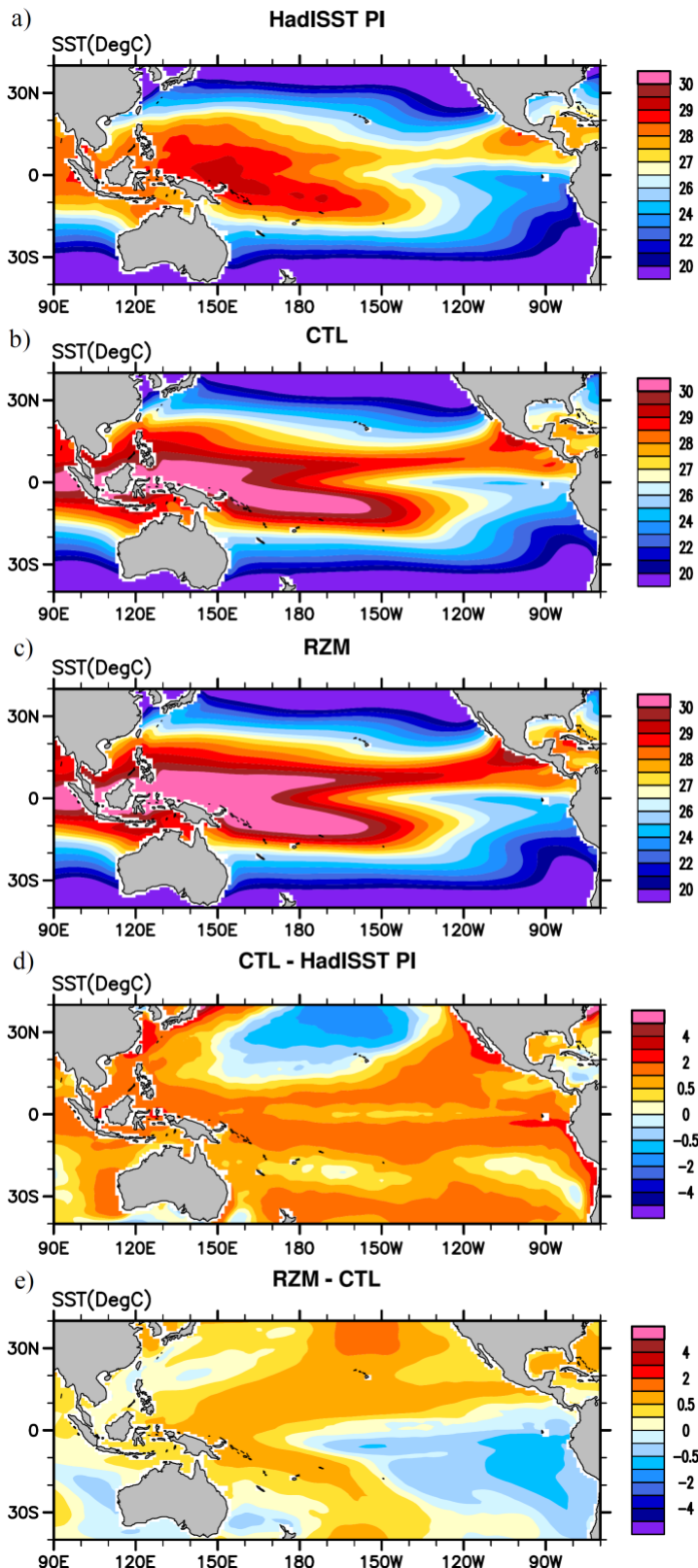
353
 354 Figure 3 zonal-pressure cross section of annual mean pressure vertical velocity (0.5 mb day^{-1}) and
 355 streamlines from ERA5, CTL, RZM, and the difference between RZM and CTL, averaged over the
 356 southern ITCZ region (2°S - 10°S).
 357

358 Previous studies attributed the double-ITCZ precipitation bias to the low-level cloud bias
 359 in the southeastern Pacific. Fig.4 evaluates the annual mean low-level cloud simulations from
 360 RZM and CTL. Compared to CALIPSO-GOCCP observations, the CTL underestimates the low-
 361 level cloud fraction by up to 40% in the southeastern Pacific. With the modified convective closure,
 362 the low-level cloud fraction is increased by up to 20% in the southeastern Pacific. Correspondingly,
 363 the shortwave cloud forcing (not shown) in the same region is increased by up to 20 W m^{-2} in RZM,
 364 which would contribute to SST cooling there.



365

366 Figure 4 Annual mean low-level cloud fraction (%) from CALIPSO-GOCCP, CTL, RZM and their
 367 differences.



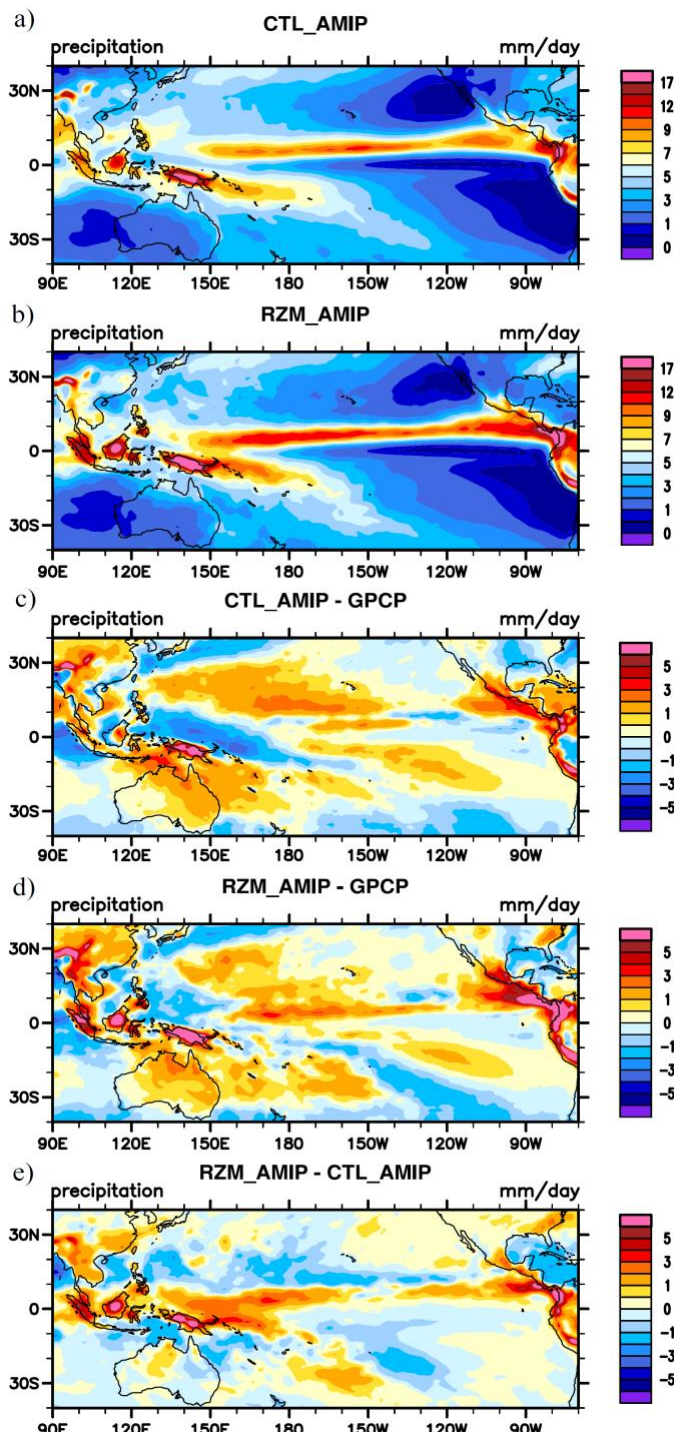
368

369 Figure 5 Annual mean sea surface temperature (SST) from HadISST, CTL, RZM, and their
370 differences.

371 Figure 5 presents the annual mean SST from HadISST, the CTL and RZM simulations,
372 along with their differences. The average SST from HadISST between 1870 and 1900 is used as
373 observed PI climatology. It shows warm SST in the tropical western Pacific warm pool and cold
374 SST in the tropical southeastern Pacific. The tropical western Pacific warm pool, an area where
375 SST is higher than 28°C, coincides with the SPCZ precipitation region south of the equator,
376 demonstrating that SST may substantially modulate deep convection. Corresponding to the overly
377 strong southern ITCZ convection as manifested by the excessive precipitation, the CTL simulates
378 a warm SST bias by up to 2°C between 2°S and 10°S in the Pacific Ocean. With the revised
379 convective closure, the RZM simulates colder SST by up to 1°C than CTL between 2°S and 10°S
380 in the Pacific Ocean, corresponding to the elimination of the precipitation bias in the southern
381 ITCZ region.

382 The SST difference between RZM and CTL in the southern ITCZ region indicates that the
383 revised convective closure triggers atmosphere-ocean feedback, which reduces the warm SST bias
384 in the southern ITCZ region and hence eliminates the double-ITCZ bias in precipitation. To verify
385 the important roles of SST change and associated coupled feedback, Fig.6 shows the annual mean
386 precipitation bias simulated by the CTL_AMIP and RZM_AMIP. Compared to the CTL, the
387 CTL_AMIP simulates very weak double-ITCZ biases in the central Pacific and does not simulate
388 double ITCZ biases in the eastern Pacific, demonstrating that the atmosphere-ocean feedback and
389 associated SST changes play critical roles in the formation of the double ITCZ bias. Compared to
390 the CTL_AMIP, the RZM_AMIP simulates stronger convection in the western Pacific and weaker
391 convection in the central Pacific between 2°S and 10°S. How do these changes induced by the
392 revised closure influence the atmosphere-ocean feedback and SST changes in RZM, and hence

393 influence the double-ITCZ bias? We conduct coupled feedback analyses in the next section to
 394 answer this question.



395
 396 Figure 6 Annual mean precipitation (mm day^{-1}) from CTL_AMIP, RZM_AMIP, and their
 397 difference (RZM_AMIP-CTL_AMIP). Annual mean precipitation biases relative to GPCP from
 398 CTL_AMIP (CTL_AMIP-GPCP) and RZM_AMIP (RZM_AMIP-GPCP).

399

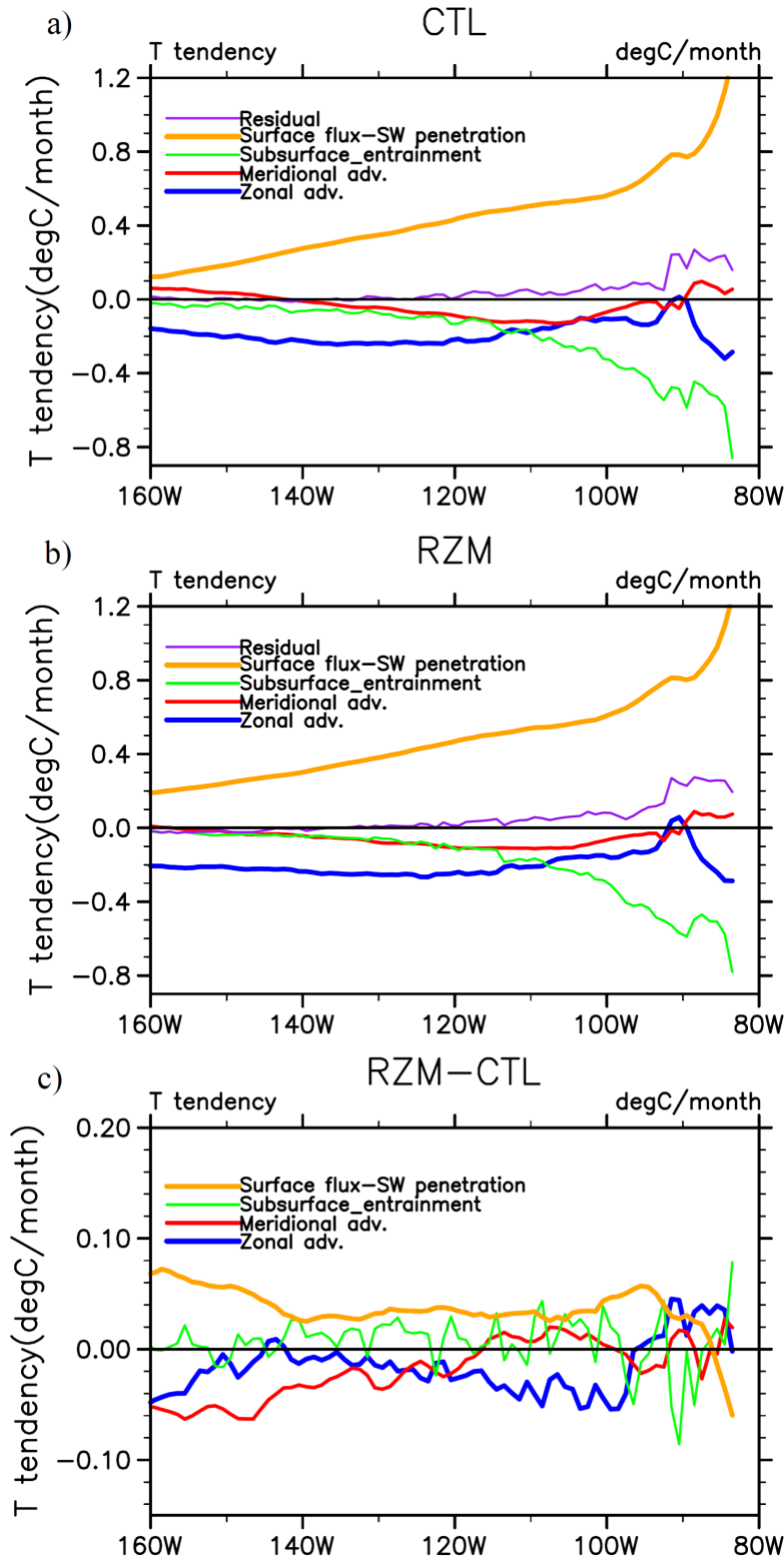
400 **4. Coupled feedback analyses**

401

402 To understand how the change in the convective scheme in atmosphere model leads to SST
 403 cooling in ocean model in the southern ITCZ region, we first perform a heat budget analysis of the
 404 ocean mixed layer in the southern ITCZ region. The temperature equation for the ocean mixed
 405 layer can be written as (Moisan and Niiler, 1998):

$$406 \quad \frac{\partial T_a}{\partial t} = \frac{Q - Q_s(-h)}{\rho c_p h} - u_a \frac{\partial T_a}{\partial x} - v_a \frac{\partial T_a}{\partial y} - \frac{(T_a - T_{-h})}{h} (w_e + w_{-h}) + R \quad (1)$$

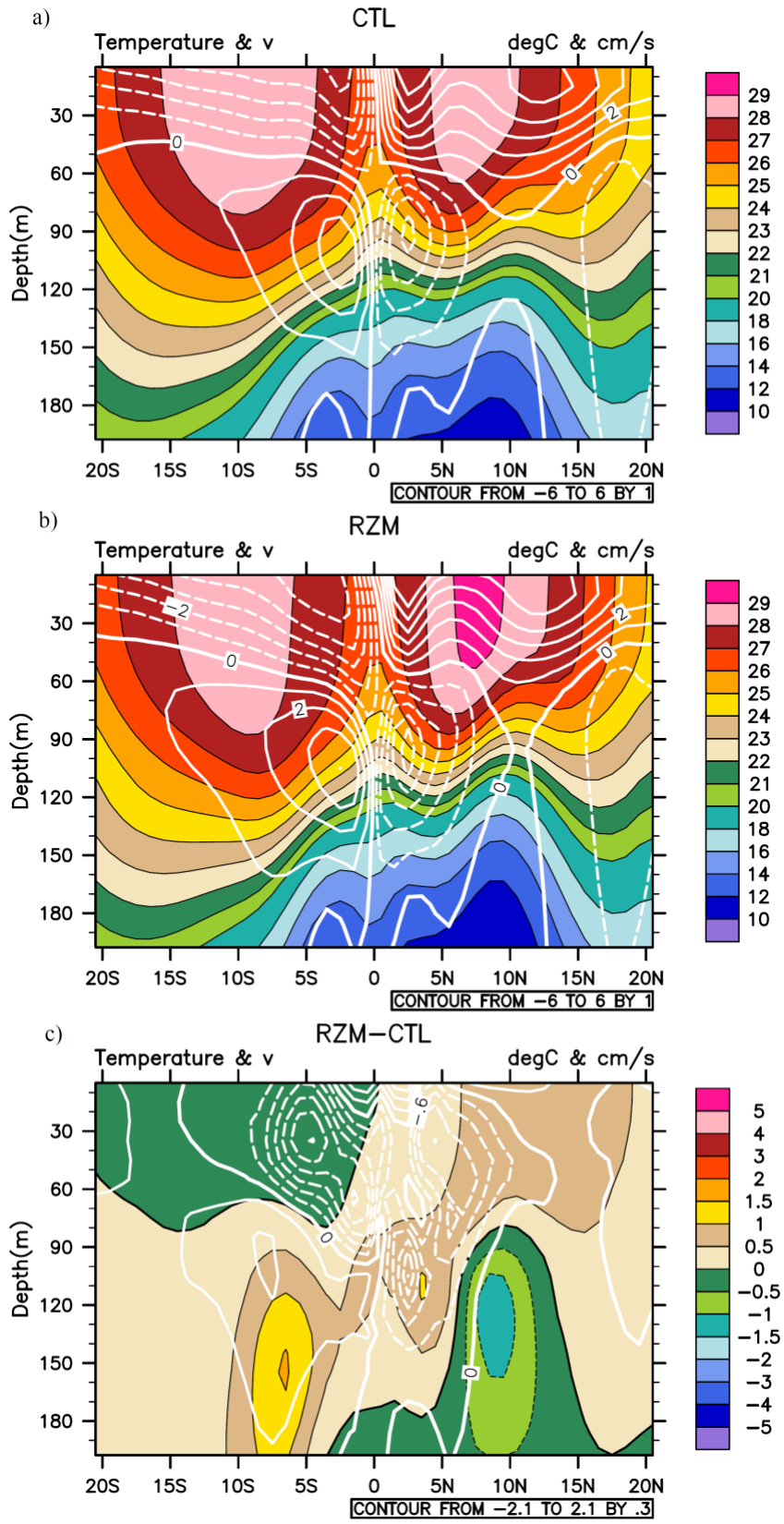
407 where T , u , and v represent temperature, zonal and meridional currents velocities in mixed layer,
 408 respectively. Subscript a represents the vertical average over the mixed layer depth h . Q is the net
 409 surface energy flux into the top of mixed layer, and $Q_s(-h)$ is the shortwave radiative flux
 410 penetrating through the base of the mixed layer. ρ [1026 kg m⁻³] is the reference density of
 411 seawater, and c_p [3996 J kg⁻¹ K⁻¹] is the specific heat of seawater at constant pressure. T_{-h} is the
 412 temperature just below the mixed layer. $w_e + w_{-h}$ is the entrainment velocity, where $w_e = \frac{dh}{dt} =$
 413 $\frac{\partial h}{\partial t} + u_{-h} \frac{\partial h}{\partial x} + v_{-h} \frac{\partial h}{\partial y}$, u_{-h} and v_{-h} are the zonal and meridional current velocities at the mixed
 414 layer base, respectively. w_{-h} is the vertical current velocity at the mixed layer base. On the right-
 415 hand side of Eq. (1), the first four terms represent the temperature changes due to net energy flux
 416 into the mixed layer, zonal advection, meridional advection, and vertical entrainment, respectively.
 417 The fifth term, R , represents the residual term, which consists of the integral of the vertical
 418 temperature-velocity covariance and horizontal diffusion.



419

420 Figure 7 Annual mean temperature tendencies of the ocean mixed layer averaged over the southern
 421 ITCZ region (2°S-10°S) from each term on the right-hand side of Eq. (1) for a) CTL, b) RZM, and
 422 c) the difference between RZM and CTL.

423 The ocean mixed layer heat budget analysis is performed using monthly mean data from
424 the model simulations following Liu et al. (2012). Figure 7 shows the annual mean of temperature
425 tendencies contributed by each term to the mixed layer temperature in the southern ITCZ region
426 (2°S-10°S). The residual terms in both CTL and RZM are very close to zero in the central and
427 eastern Pacific from 160°W to 90°W. Near the coast, the residual terms are increased slightly but
428 are still much smaller than the major warming/cooling terms. These demonstrate that the heat
429 budget analysis is reasonably accurate. In both CTL and RZM, the major heating term for the
430 ocean mixed layer is the surface heat flux, primarily balanced by cooling due to zonal advection,
431 which transports cold water from east to west between 110°W to 160°W. East of 110°W, the
432 cooling due to vertical entrainment of cold water at the base of the mixed layer (i.e., upwelling of
433 cold water) plays more important role. The difference between RZM and CTL suggests that the
434 SST cooling in RZM is caused by different terms in different regions. In the central Pacific
435 between 120°W and 160°W, the major cooling term is meridional advection, with some
436 contribution from zonal advection between 150°W and 160°W. Zonal advection is the dominant
437 cooling term between 100°W and 120°W. Vertical entrainment contributes to the SST cooling near
438 90°W, while the surface heat flux only produces cooling east of 87°W.



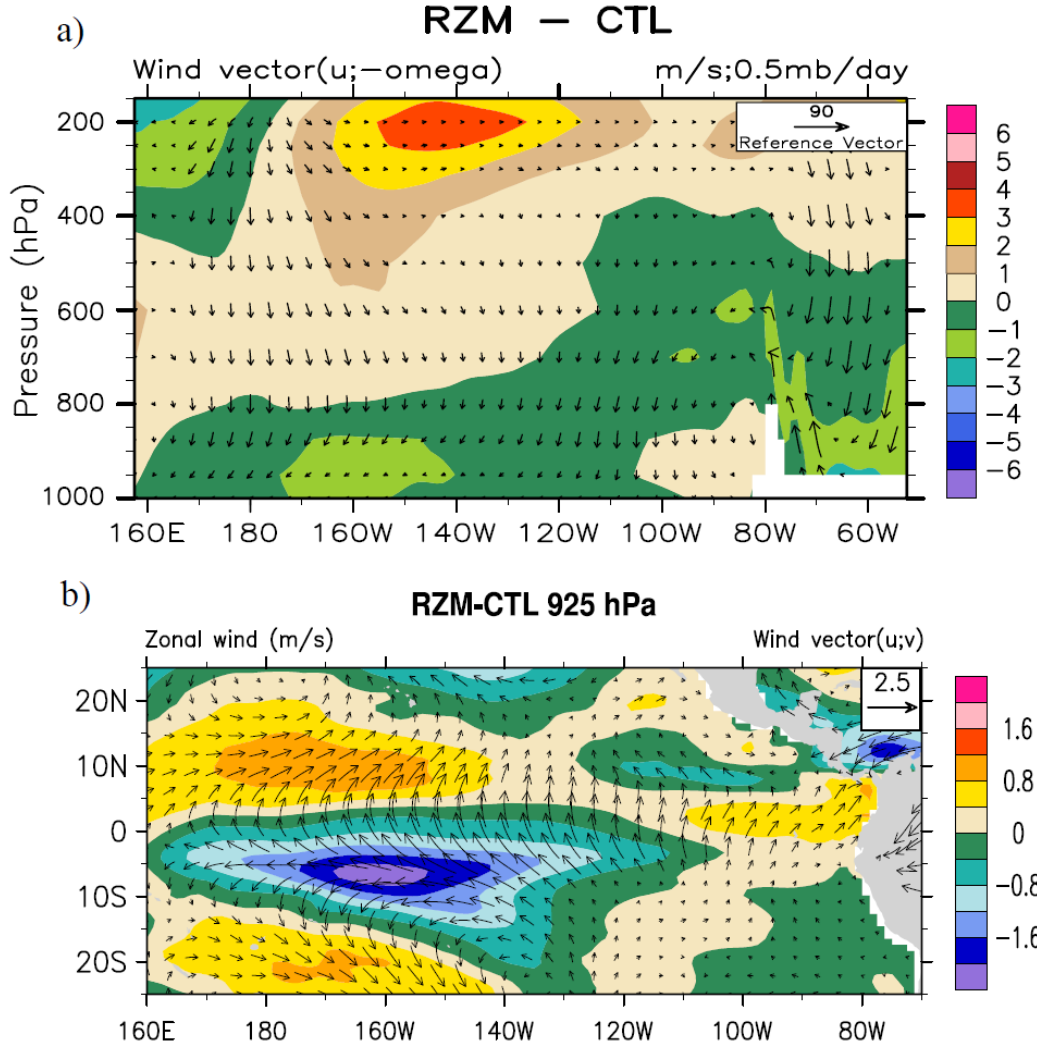
439

440 Figure 8 Annual mean upper ocean temperature (°C) and meridional current averaged over 120°W-
 441 160°W from a) CTL, b) RZM, and c) the difference between RZM and CTL.

442 To understand the mechanism through which meridional advection cools the SST in RZM
443 in the central Pacific, Fig.8 presents the latitude-depth diagram of ocean temperature and
444 meridional currents from RZM and CTL averaged over 120°W-160°W. Corresponding to the
445 equatorial upwelling, equatorward currents below 50m generates mass convergence near the
446 equator, while the poleward currents in the upper 50m produce mass divergence from the equator
447 and cold meridional temperature advection to the southern ITCZ region. The difference between
448 RZM and CTL clearly shows that mass divergence is enhanced in the upper 20m near 2°S,
449 indicating the upwelling is enhanced in the RZM in the central Pacific. Since the equatorial
450 upwelling is driven by surface wind, we further examine changes in zonal wind (shaded) and wind
451 vectors from CTL to RZM in the atmospheric model averaged between 5°S and the equator in the
452 longitude-height plane.

453 Fig.9a shows that the subsidence and low-level easterlies are enhanced in RZM in the
454 equatorial central Pacific between 120°W and 160°W. The zonal wind speed and wind vector (u ,
455 v) differences between RZM and CTL at 925 hPa (Fig. 9b) further illustrate that the low-level
456 easterlies are increased in the central Pacific over the southern ITCZ region. This is consistent with
457 Fig.3, indicating that the Walker circulation is enhanced in RZM. This circulation change in RZM
458 coincides with the precipitation (convection) change as shown in Fig.2, where convection is
459 suppressed over equatorial central and eastern Pacific and enhanced over equatorial western
460 Pacific in RZM.

461



462

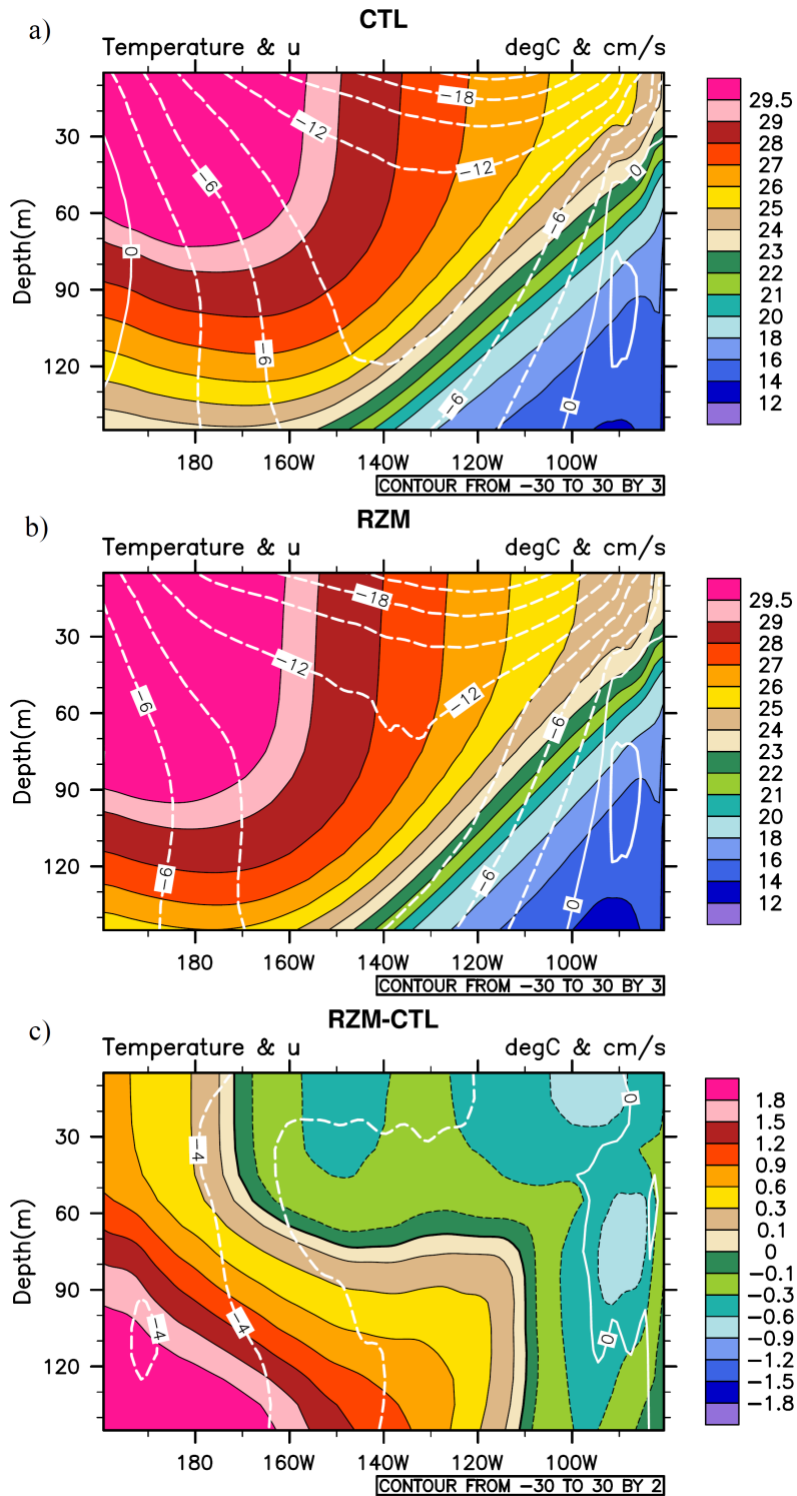
463 Figure 9 a) Zonal-pressure cross section of differences in annual mean zonal wind (m s^{-1} , shaded)
 464 and wind vectors ($u: \text{m s}^{-1}$; $\omega: 0.5 \text{ mb day}^{-1}$) between RZM and CTL, averaged over (0° - 5°S).
 465 b) corresponding zonal wind speed and wind vector (u ; v) differences between RZM and CTL at
 466 925 hPa.

467 The convection changes in the coupled simulation introduced by the modified convective
 468 closure can be traced back to the AMIP simulation (Fig.6), which shows the modified convective
 469 closure tends to suppress convection in the central and eastern Pacific and enhance convection in
 470 the western Pacific. Therefore, the coupled feedback mechanism through which the modified
 471 convective closure mitigates the double-ITCZ bias in the central Pacific can be summarized as
 472 follows: The modified convective closure tends to suppress convection in the central Pacific. The

473 low-level easterly then transports more water vapor to the western Pacific and enhances convection
474 there. The convection changes strengthen Walker circulation and increase descending motion and
475 low-level easterly in the central Pacific, which in turn suppress convection in the central Pacific
476 and enhance convection in the western Pacific. In addition, the resultant increase in the surface
477 easterly in the equatorial central Pacific may enhance equatorial upwelling in the ocean and
478 produce stronger meridional divergence in the upper ocean. The enhanced poleward currents
479 transport cold water to the southern ITCZ region and reduce SST there. The colder SST in the
480 southern ITCZ region in the central Pacific may further suppress convection there and resultant
481 feedback leads to the mitigation of double-ITCZ bias in the central Pacific.

482 To understand the role of changes in zonal temperature advection in the upper ocean in
483 mitigating the double-ITCZ bias in the southern ITCZ region, Fig.10 presents the longitude-depth
484 diagram of ocean temperature (shaded) and zonal currents averaged over 2°S-10°S from CTL and
485 RZM, along with their differences. The ocean temperature gradually increases from the eastern to
486 western Pacific. Corresponding to the surface easterly wind, the westward surface currents
487 transport cold water from the eastern Pacific to the western Pacific, leading to cold temperature
488 advection. The difference between RZM and CTL shows that both enhanced zonal currents and
489 temperature gradient in RZM contribute to the increased cooling due to zonal temperature
490 advection. The strengthening of zonal current can be attributed to the enhanced surface easterlies,
491 as shown in Fig.3. As demonstrated in the ocean mixed layer heat budget analysis, the enhanced
492 zonal temperature advection is the major contributor to the SST cooling in RZM between 100°W
493 and 120°W, where the zonal gradient of ocean temperature is notably increased. The deep cooling
494 of temperature from 140 m to the ocean surface east of 100°W indicates that the enhanced

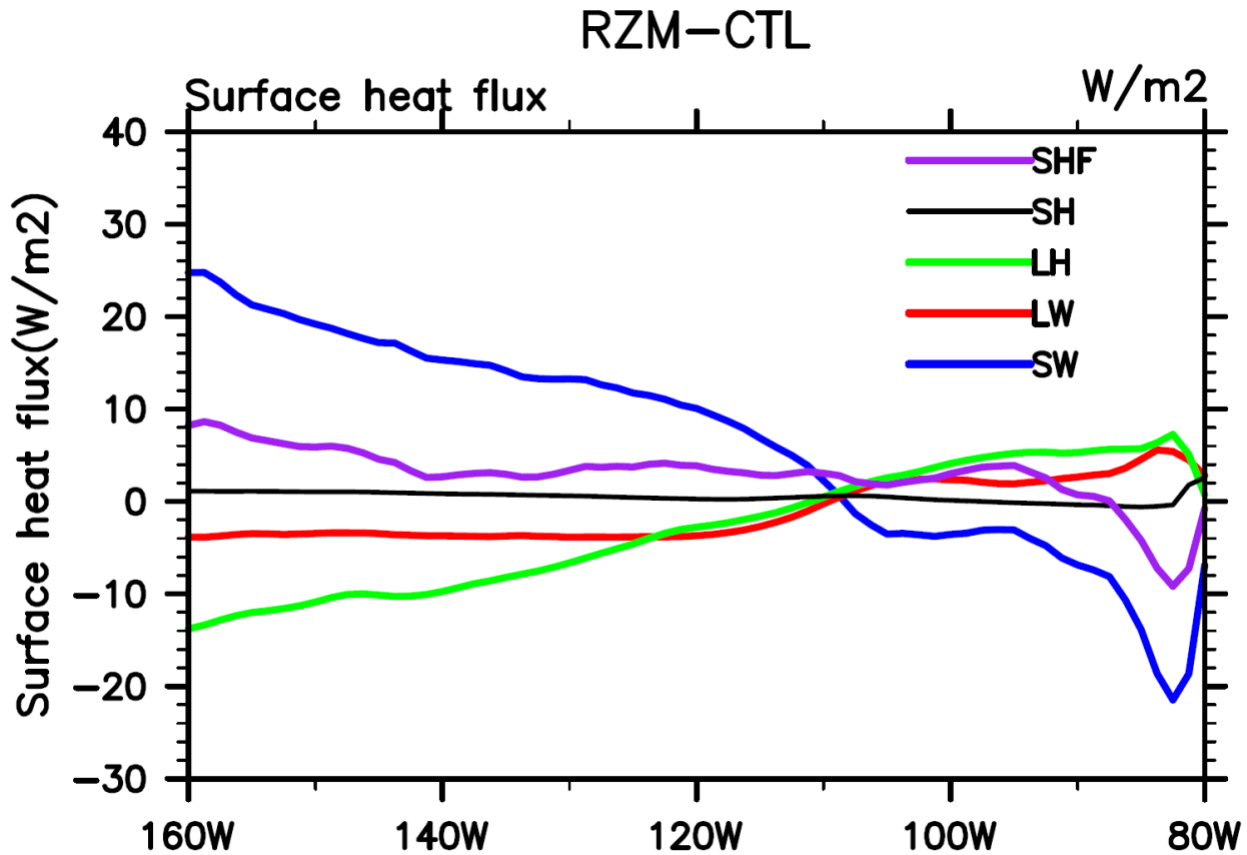
495 upwelling east of 100°W may contribute to the increased temperature gradient between 100°W
 496 and 120°W.



497
 498 Figure 10 Annual mean upper ocean temperature (°C) and zonal current (cm s⁻¹) averaged over
 499 2°S-10°S from a) CTL, b) RZM, and c) the difference between RZM and CTL.

500 As discussed in Section 3, the modified convective closure improves the low-level cloud
501 and shortwave cloud radiative forcing in the southeastern Pacific, which could result in SST
502 cooling in RZM. However, the heat budget analysis of the ocean mixed layer shows that the change
503 of net heat flux into the ocean mixed layer (the first term on the right-hand side of Eq. 1) in RZM
504 only contributes to SST cooling in a very limited region (82°W - 87°W) in the equatorial
505 southeastern Pacific. Since the net surface heat flux into the mixed layer at the sea surface
506 represents the net effect of its four components: shortwave radiative flux, longwave radiative flux,
507 sensible heat and latent heat flux, we further analyze the contribution of these four components to
508 the net surface heat flux change in RZM. Figure 11 shows the annual mean difference in the surface
509 heat flux (into the ocean) components between RZM and CTL, averaged over 2°S - 10°S .
510 Comparing to CTL, the net surface heat flux into the ocean in RZM is increased slightly across the
511 central and eastern Pacific from 160°W to 87°W and decreased over 87°W - 82°W , indicating that
512 the net surface heat flux changes in RZM may induce SST warming in most of the southern ITCZ
513 region and only contribute to SST cooling in the region over 87°W - 82°W . This also suggests that
514 the changes in the other two factors in the net heat flux term of Eq. (1): mixed layer depth and
515 shortwave radiative flux penetrating through the base of the mixed layer, have little impact on the
516 SST change in RZM. The shortwave radiative flux into the ocean is increased in the region 110°W -
517 160°W in RZM due to reduced convection and cloud, while it is decreased in the region 110°W -
518 82°W because of the increase of low-level cloud. However, the net longwave radiative flux out of
519 the ocean is also decreased (decrease in upward heat flux is equivalent to an increase in downward
520 heat flux or relative heating) over 110°W - 82°W due to the increase in low-level cloud.
521 Additionally, the latent heat flux out of the ocean is decreased (thus less cooling or relatively more
522 heating) due to weaker wind speeds. As a result, the net surface heat flux change in RZM only

523 contributes to SST cooling in a very limited region (82°W - 87°W) in the equatorial southeastern
524 Pacific.



525
526 Figure 11 Differences in components of annual mean surface heat flux into the ocean: net surface
527 heat flux (SHF), sensible heat flux (SH), latent heat flux (LH), longwave radiative heat flux (LW),
528 and shortwave radiative flux (SW) between RZM and CTL, averaged over 2°S - 10°S . All fluxes
529 are defined as positive downward (into the ocean).

530 **5. Summary and conclusions.**

531 In this study, we examined the impact of convective closure on the double-ITCZ bias in
532 the NCAR CESM2.2. Although the model development from CESM1.2 to CESM2.2 has
533 significantly reduced the dry tongue bias over the equator and the excessive precipitation bias in
534 the southern ITCZ region between 120°W and 150°W , the standard CESM2.2 still simulates a
535 remarkable double-ITCZ bias in the central and eastern Pacific. In the spring, the simulated

536 southern ITCZ is even stronger than the northern ITCZ, forming a reversed interhemispheric
537 asymmetry. The revised convective closure greatly reduces the double-ITCZ bias in all seasons,
538 demonstrating that convection parameterization can substantially influence the double-ITCZ bias
539 in CESM2.2. It should be noted that the same closure change in CESM1.2.1 can only eliminate
540 the double-ITCZ bias in summer and autumn, suggesting that other model process
541 parameterizations, such as the cloud microphysics scheme and PBL scheme, may also contribute
542 to the coupled feedback that influences the double-ITCZ bias. However, this study demonstrates
543 that convection parameterization is one of the most important processes that can substantially
544 influence the double-ITCZ bias.

545 The atmospheric model simulation of CESM2.2 forced by observed SST simulates a very
546 weak double ITCZ bias in the central Pacific and does not simulate a double ITCZ bias in the
547 eastern Pacific, demonstrating that the atmosphere–ocean feedback and associated SST changes
548 play critical roles in the formation of the double-ITCZ bias. The fully coupled simulation of
549 CESM2.2 produced warm SST biases in the southern ITCZ region, while the coupled simulation
550 with modified convective closure significantly reduced the warm SST biases, indicating that
551 convection parameterization in the atmosphere model can influence the ocean SST and double-
552 ITCZ bias in precipitation through coupled feedback processes.

553 To understand how the convection parameterization scheme change in the atmosphere
554 model leads to SST cooling in the ocean model in the southern ITCZ region, we perform the heat
555 budget analysis of the ocean mixed layer in the southern ITCZ region. It shows that the modified
556 convective closure introduces SST cooling through several mechanisms, each of which is
557 dominant in different regions. In the central Pacific between 120°W-160°W, the major cooling is
558 caused by meridional advection changes, with some contribution from zonal advection between

559 150°W and 160°W. Further analysis suggests that the convective closure may influence the double-
560 ITCZ bias through the following mechanism: The modified convective closure tends to suppress
561 convection in the central Pacific. The low-level easterly then transports more water vapor to the
562 western Pacific and enhances convection there. The changes in convection strengthen the Walker
563 circulation and increase descending motion and low-level easterly winds in the central Pacific,
564 which, in turn, suppress convection in the central Pacific and enhance convection in the western
565 Pacific. Additionally, the resultant increase in surface easterly winds in the equatorial central
566 Pacific may enhance upwelling in the ocean and produce stronger meridional divergence in the
567 upper ocean. The enhanced poleward currents transport cold water to the southern ITCZ region
568 and reduce SST there. The colder SST in the southern ITCZ region in the central Pacific may
569 further suppress convection there, and the resultant feedback leads to the mitigation of the double-
570 ITCZ bias in the central Pacific.

571 Between 100°W and 120°W, when the modified convective closure is used, the enhanced
572 surface easterly wind drives stronger westward surface currents, which transport more cold water
573 from the eastern Pacific to the central Pacific, resulting in the SST cooling in the southern ITCZ
574 region. In this region, the zonal gradient of ocean temperature is also notably increased, which can
575 be attributed to the enhanced upwelling east of 100°W.

576 Although the modified convective closure improves the low-level cloud and shortwave
577 cloud radiative forcing in the southeastern Pacific, the surface heat flux only contributes to SST
578 cooling in a very limited region (82°W-87°W) in the equatorial southeastern Pacific because the
579 impacts shortwave radiation changes are largely canceled by changes in longwave radiation and
580 latent heat flux.

581 In summary, this study demonstrates that convection parameterization substantially
582 influences the double-ITCZ bias in CESM2.2 by modulating the coupled feedback, in which the
583 equatorial upper ocean processes play important roles, while the could-radiation processes in
584 equatorial southeastern Pacific play a limited role.

585

586 **Acknowledgments**

587 This research was supported by the National Science Foundation Grant AGS-2054697, and
588 by U.S. Department of Energy's (DOE's) Earth System Model Development and Analysis
589 (ESMDA) program under Award Numbers DE-SC0022064 and DE-SC0023069

590 **Data Availability Statement**

591 The observational datasets used in this study are available at:
592 <https://web.lcrc.anl.gov/public/e3sm/diagnostics/observations/Atm/climatology/>. The simulation
593 data used in this study can be found on Zenodo at <https://zenodo.org/records/10702744>.

594

595

596

597

598

599

600

601 **References:**

602 Chepfer, H., S. Bony, D. Winker, G. Cesana, J. L. Dufresne, P. Minnis, C. J. Stubenrauch, and S.
603 Zeng (2010), The GCM-Oriented CALIPSO Cloud Product (CALIPSO-GOCCP),
604 Journal of Geophysical Research , 115, D00H16, doi:10.1029/2009JD012251.

605 Danabasoglu, G., Lamarque, J.-F., Bacmeister, J., Bailey, D. A., DuVivier, A. K., Edwards, J., et
606 al. (2020). The Community Earth System Model Version 2 (CESM2). Journal of
607 Advances in Modeling Earth Systems, 12, e2019MS001916.
608 <https://doi.org/10.1029/2019MS001916>

609 Gettelman, A., Morrison, H., Santos, S., Bogenschutz, P., & Caldwell, P. M. (2015). Advanced
610 two - moment bulk microphysics for global models. Part II: Global model solutions and
611 aerosol - cloud interactions. Journal of Climate, 28(3), 1288 – 1307.
612 <https://doi.org/10.1175/JCLI-D-14-00103.1>

613 Hawcroft, M., Haywood, J.M., Collins, M., Jones, A., Jones, A. C., & Stephens, G. (2017).
614 Southern Ocean albedo, inter-hemispheric energy transports and the double ITCZ: Global
615 impacts of biases in a coupled model. Climate Dynamics, 48, 2279 – 2295.
616 <https://doi.org/10.1007/s00382-016-3205-5>

617 Herrington, A. R., Lauritzen, P. H., Lofverstrom, M., Lipscomb, W. H., Gettelman, A., &
618 Taylor, M. A. (2022). Impact of grids and dynamical cores in CESM2.2 on the surface
619 mass balance of the Greenland Ice Sheet. Journal of Advances in Modeling Earth
620 Systems, 14, e2022MS003192. <https://doi.org/10.1029/2022MS003192>

621 Hersbach H, Bell B, Berrisford P, et al. The ERA5 global reanalysis. *Q J R Meteorol Soc.* 2020;
622 146: 1999–2049. <https://doi.org/10.1002/qj.3803>

623 Huffman, G. J., R. F. Adler, A. Behrangi, D. T. Bolvin, E. J. Nelkin, G. Gu, and M. R. Ehsani,
624 2023: The New Version 3.2 Global Precipitation Climatology Project (GPCP) Monthly
625 and Daily Precipitation Products. *Journal of Climate*, 36, 7635–7655,
626 <https://doi.org/10.1175/JCLI-D-23-0123.1>.

627 Hwang, Y.-T. & Frierson, D.M.W. (2013) Link between the double-intertropical convergence
628 zone problem and cloud biases over the Southern Ocean. *Proceedings of the National
629 Academy of Sciences*, 110, 4935–4940. <https://doi.org/10.1073/pnas.1213302110>

630 Kang, S.M. (2020) Extratropical influence on the tropical rainfall distribution. *Curr. Clim.
631 Chang. Reports*, 6, 24–36. <https://doi.org/10.1007/s40641-020-00154-y>

632 Kato, S., Rose, F. G., Rutan, D. A., Thorsen, T. J., Loeb, N. G., Doelling, D. R., Huang, X.,
633 Smith, W. L., Su, W., and Ham, S.-H. (2018). Surface irradiances of edition 4.0 Clouds
634 and the Earth’s Radiant Energy System (CERES) Energy Balanced and Filled (EBAF)
635 data product, *Journal of Climate*, 31, 4501–4527.

636 Kawai, Hideaki & Koshiro, Tsuyoshi & Yukimoto, Seiji. (2021). Relationship between
637 shortwave radiation bias over the Southern Ocean and the double - intertropical
638 convergence zone problem in MRI - ESM2. *Atmospheric Science Letters*. 22.
639 10.1002/asl.1064.

640 Kay, J. E., Wall, C., Yettella, V., Medeiros, B., Hannay, C., Caldwell, P., et al. (2016). Global
641 climate impacts of fixing the Southern Ocean short-wave radiation bias in the

Community Earth System Model (CESM). *Journal of Climate*,
<https://doi.org/10.1175/JCLI-D-15-0358.1>

Kim, Hanjun, Kang, Sarah M., Kay, Jennifer E., & Xie, Shang-Ping (2022). Subtropical clouds
key to Southern Ocean teleconnections to the tropical Pacific. *Proceedings of the
National Academy of Sciences* 119 (34). <https://doi.org/10.1073/pnas.2200514119>.
<https://par.nsf.gov/biblio/10384370>.

Lin, J. L. (2007). The double-ITCZ problem in IPCC AR4 coupled GCMs: Ocean-atmosphere
feedback analysis. *Journal of Climate*, 20(18), 4497 – 4525.
<https://doi.org/10.1175/JCLI4272.1>

Liu, H., Zhang, M., & Lin, W. (2012). An investigation of the initial development of the double-
ITCZ warm SST biases in the CCSM. *Journal of Climate*, 25, 140–155,
<https://doi.org/10.1175/2011JCLI4001.1>

Lee, J., Kang, S. M., Kim, H., and Xiang, B. (2022). Disentangling the effect of regional SST
bias on the double-ITCZ problem. *Climate Dynamics*, 58, 3441–3453.
doi:10.1007/s00382-021-06107-x.

Ma, C. C., Mechoso, C. R., Robertson, A. W., & Arakawa, A. (1996). Peruvian stratus clouds
and the tropical Pacific circulation: A coupled ocean-atmosphere study. *Journal of
Climate*, 9, 1635–1645.

Ma, X., Zhao, S., Zhang, H., & Wang, W. (2023). The double-ITCZ problem in CMIP6 and the
influences of deep convection and model resolution. *International Journal of
Climatology*, 43(5), 2369–2390. <https://doi.org/10.1002/joc.7980>

663 Mechoso, C.R., Robertson, A.W., Barth, N., Davey, M.K., Delecluse, P., Gent, P.R. et al. (1995)

664 The seasonal cycle over the tropical Pacific in coupled ocean–atmosphere general

665 circulation models. *Monthly Weather Review*, 123, 2825–2838.

666 [https://doi.org/10.1175/1520-0493\(1995\)123<2825:TSCOTT>2.0.CO;2](https://doi.org/10.1175/1520-0493(1995)123<2825:TSCOTT>2.0.CO;2)

667 Mechoso, C.R., Losada, T., Koseki, S., Mohino-Harris, E., Keenlyside, N., Castaño-Tierno, A. et

668 al. (2016) Can reducing the incoming energy flux over the Southern Ocean in a CGCM

669 improve its simulation of tropical climate? *Geophysical Research Letters*, 43, 11057–

670 11063. <https://doi.org/10.1002/2016GL071150>

671 Moisan, J. R., & Niiler, P. P. (1998). The Seasonal Heat Budget of the North Pacific: Net Heat

672 Flux and Heat Storage Rates (1950–1990). *J. Phys. Oceanogr.*, 28, 401–421,

673 [https://doi.org/10.1175/1520-0485\(1998\)028<0401:TSHBOT>2.0.CO;2](https://doi.org/10.1175/1520-0485(1998)028<0401:TSHBOT>2.0.CO;2).

674 Neale, R. B., Richter, J. H., & Jochum, M. (2008). The impact of convection on ENSO: From a

675 delayed oscillator to a series of events. *Journal of Climate*, 21, 5904 – 5924.

676 Rayner, N. A., Parker, D. E., Horton, E. B., Folland, C. K., Alexander, L. V., Rowell, D. P., &

677 Kaplan, A. (2003). Global analyses of sea surface temperature, sea ice, and night marine

678 air temperature since the late nineteenth century. *Journal of Geophysical Research*,

679 108(D14), 4407. <https://doi.org/10.1029/2002JD002670>

680 Song, F., & Zhang, G. J. (2016). Effects of southeastern Pacific sea surface temperature on the

681 double-ITCZ bias in NCAR CESM1. *Journal of Climate*, 29, 7417 – 7433.

682 <https://doi.org/10.1175/JCLI-D-15-0852.1>

683 Song, X., & Zhang, G. J. (2009). Convection parameterization, tropical Pacific double ITCZ, and
684 upper-ocean biases in the NCAR CCSM3. Part I: Climatology and atmospheric feedback.
685 Journal of Climate, 22, 4299 – 4315. <https://doi.org/10.1175/2009JCLI2642.1>

686 Song, X., & Zhang, G. J. (2018). The roles of convection parameterization in the formation of
687 double ITCZ syndrome in the NCAR CESM: I. Atmospheric processes. Journal of
688 Advances in Modeling Earth Systems, 10. <https://doi.org/10.1002/2017MS001191>

689 Tian, B. & Dong, X. (2020) The double-ITCZ bias in CMIP3, CMIP5, and CMIP6 models based
690 on annual mean precipitation. Geophysical Research Letters, 47, 1–11.
691 <https://doi.org/10.1029/2020GL087232>

692 Woelfle, M. D., Bretherton, C. S., Hannay, C., & Neale, R. (2019). Evolution of the double-
693 ITCZ bias through CESM2 development. Journal of Advances in Modeling Earth
694 Systems, 11, 1873 – 1893. <https://doi.org/10.1029/2019MS001647>

695 Xiang, B., Zhao, M., Held, I. M., & Golaz, J.-C. (2017). Predicting the severity of spurious
696 "double ITCZ" problem in CMIP5 coupled models from AMIP simulations. Geophysical
697 Research Letters, 44(3), 1520-1527.

698 Xie, S., Wang, Y.-C., Lin, W., Ma, H.-Y., Tang, Q., Tang, S., et al. (2019). Improved diurnal
699 cycle of precipitation in E3SM with a revised convective triggering function. Journal of
700 Advances in Modeling Earth Systems, 11, 2290–2310.
701 <https://doi.org/10.1029/2019MS001702>

702 Yu, J.-Y., & Mechoso, C. R. (1999). Links between annual variations of Peruvian stratocumulus
703 clouds and of SST in the eastern equatorial Pacific. Journal of Climate, 12, 3305 – 3318.

704 Zhang, C. (2001). Double ITCZs. *Journal of Geophysical Research*, 106(D11), 11785 – 11792.

705 <https://doi.org/10.1029/2001JD900046>

706 Zhang, G. J. (2002). Convective quasi - equilibrium in midlatitude continental environment and
707 its effect on convective parameterization. *Journal of Geophysical Research*, 107(D14),
708 4220. <https://doi.org/10.1029/2001JD001005>

709 Zhang, G. J., & McFarlane, N. A. (1995). Sensitivity of climate simulations to the parameterization
710 of cumulus convection in the Canadian Climate Centre general circulation model.
711 *Atmosphere-Ocean*, 33, 407 – 446. <https://doi.org/10.1080/07055900.1995.9649539>

712 Zhang, G. J., & Song, X. (2010). Convection parameterization, tropical Pacific double ITCZ, and
713 upper-ocean biases in the NCAR CCSM3. Part II: Coupled feedback and the role of ocean
714 heat transport. *Journal of Climate*, 23, 800 – 812.
715 <https://doi.org/10.1175/2009JCLI3109.1>

716 Zhang, G. J. & Wang, H. (2006). Toward mitigating the double ITCZ problem in NCAR CCSM3.
717 *Geophysical Research Letters*, 33. 10.1029/2005GL025229.

718 Zhang, X., Liu, H., & Zhang, M. (2015). Double ITCZ in Coupled Ocean-Atmosphere Models:
719 From CMIP3 to CMIP5. *Geophysical Research Letters*, 42, 8651 – 8659.
720 <https://doi.org/10.1002/2015GL065973>

721 Zhou, W., Leung, L. R., & Lu, J. (2022). Linking Large-Scale Double-ITCZ Bias to Local-Scale
722 Drizzling Bias in Climate Models. *Journal of Climate*, 35(24), 7965-7979.

723 Zhou, W., & Xie, S.-P. (2017). Intermodel spread of the double-ITCZ bias in coupled GCMs tied
724 to land surface temperature in AMIP GCMs. *Geophysical Research Letters*, 44(15), 7975-
725 7984.